THE JOURNAL OF PHYSICAL CHEMISTRY B

Article

pubs.acs.org/JPCB

Displacements, Mean-Squared Displacements, and Codisplacements for the Calculation of Nonequilibrium Properties

Mithila V. Agnihotri,[†] Si-Han Chen,[‡] Corey Beck,[‡] and Sherwin J. Singer*[,†,‡]

[†]Biophysics Program and [‡]Department of Chemistry and Biochemistry, Ohio State University, Columbus, Ohio 43210, United States

ABSTRACT: We study two situations in which nonequilibrium phenomena can be efficiently calculated using displacements, mean-squared displacements, or codisplacements instead of accumulating velocities or currents. The flow velocity profile for a fluid confined within a pore can be expressed as a sum of displacements within slabs from a molecular dynamics trajectory. In this form, an accurate flow profile is obtained from very sparse sampling of the trajectory. We also recast the linear response theory expression for the flow velocity profile in terms of mean codisplacements and demonstrate that this provides an efficient route for estimating the Green−Kubo expression for the velocity profile. Finally, we calculate the ionic contribution to the frequency-dependent electric susceptibility using dipolar displacements, instead of the conventional current−current correlation function. We expect these methods to be useful for generating transport properties from stored trajectories in very large systems or systems where relaxation times are long.

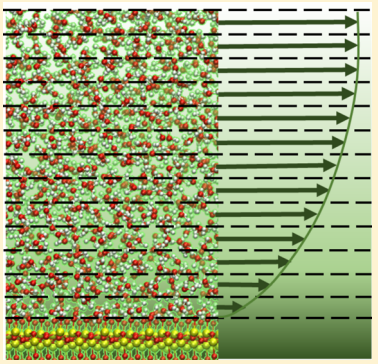

1. INTRODUCTION

Calculation of nonequilibrium properties from molecular dynamics simulations generally involves time averages. For example, one quantity of interest that has been extracted from simulations is the spatially resolved flow velocity of confined fluids under the action of an external field. The conventional approach in nonequilibrium molecular dynamics simulations is to build a flow profile by averaging molecular velocities within layers perpendicular to channel walls.[1−22] This method requires extensive averaging because room-temperature molecular velocities are typically several hundred meters per second, while flow velocities are at least an order of magnitude smaller (and must be if the linear response to the driving force is required). This can be problematic for large systems, especially if the analysis involves stored trajectory files. Simulations of electrokinetic phenomena can be similarly demanding when the flow is driven by small numbers of ions because long runs are needed for a small number of ions to fully sample available configurations. An elegant approach to the flow velocity profile was developed by Marry et al. They used linear response theory to obtain an expression for the electroosmotic flow profile in terms of velocity−velocity correlation functions.[23−25] The linear response expressions are especially demanding with respect to overcoming sampling error. In applications to date,[23−25] wide spatial bins were used, presumably to accumulate better statistics but at the expense of insufficient detail about the flow velocity profile. Even with this compromise, error bars are comparable to the desired averages.

In this work, we show that sampling statistics from limited simulation data can be dramatically improved for both nonequilibrium and linear response methods by accumulating displacements in situations where typically velocities or currents have been accumulated. The displacements are generated from an integral of the time-dependent velocity, $\int^t dt'\, \mathbf{v}(t')$, and have in the past been termed "trajectories with jumps removed",[26] or "unwrapped" trajectories.[27,28] We adopt the latter usage and refer to such trajectories as "unwrapped" trajectories in our work. The collection of unwrapped trajectories is initially confined to a simulation cell but eventually diffuse away from the cell. Such trajectories are a useful way to calculate physically meaningful quantities. Using displacements from unwrapped trajectories, sampling error is dramatically reduced, and the time interval between points at which configurations must be sampled can be greatly extended.

Employing modern molecular dynamics software, trajectory files are first generated and then subsequently processed to obtain flow profiles or response functions of interest. Extensive averaging of very large systems may be required in many situations, such as treatment of macromolecular or biomolecular complexes. Extensive averaging may also be needed when certain components are dilute. In these situations, the data files used to store the requisite trajectories may become prohibitively large. Extension of the time between sampling points has its greatest utility in this context. In the work, we demonstrate that accumulating a displacement instead of averaging a flow velocity can be orders of magnitude more efficient for estimating fluid flow.

A second area where we will explore the advantage of displacements is in the calculation of the frequency-dependent electrical susceptibility. Here, the analogue of moving from velocity to displacement is the transition from current to dipolar displacement, $\mathbf{M}_j(t) = \int^t dt'\, \mathbf{J}(t')$, as introduced by

Special Issue: James L. Skinner Festschrift

Received: February 4, 2014
Revised: April 28, 2014

 © XXXX American Chemical Society dx.doi.org/10.1021/jp5012523 | J. Phys. Chem. B XXXX, XXX, XXX−XXX

Caillol et al.[29,30] and Schröder and Steinhauser.[31] The dipolar displacement is the dipole moment of a collection of charged particles whose continuous trajectory originates within the simulation cell but eventually diffuses out of the cell. In systems of neutral polar molecules, dipole−dipole correlation functions are the preferred route to the frequency-dependent electrical response. However, the dipole is not well-defined when the system contains ions as the dipole of the primary simulation cell shifts discontinuously when an ion crosses a periodic boundary. Hence, for an electrolyte, it is standard[31−38] to accumulate a dipole−dipole correlation function for the polar solvent, a current−current correlation function for the ions, and a mixed dipole−current correlation function for the cross terms. Schröder has used fitting functions for both the current−current correlation function and the mean-square dipolar displacement.[39] In this work, we compare how both methods stand up to extending the sampling interval.

The frequency-dependent dielectric properties of biomolecules are of great interest.[40−42] The computational challenge has been recognized for predicting dielectric relaxation phenomena from molecular dynamics simulations of large biomolecules[31,43] and even smaller biomolecules like amino acids.[44] Unlike similar studies for polar fluids or electrolyte solutions, it is difficult to obtain dipole moment or current correlation functions with sufficiently low statistical error to support direct Fourier−Laplace transformation to frequency-dependent electrical susceptibility or conductivity. Instead, the prevailing approach is to smooth simulation data by fitting to either a sum of exponentials, a stretched exponential, or an oscillatory function time an exponential.[43−46] The computational demands are especially high when the biomolecule is charged, and its dipole is not well-defined. Indeed, we were motivated to develop methods that require a minimum of configurations sampled from a trajectory by working with very large systems. Without more efficient techniques, the data sets needed to extract flow velocity, or dielectric properties become unmanageable.

The paper is organized as follows. In section 2, we consider nonequilibrium molecular dynamics simulations of a fluid confined in a channel. We cast the steady-state flow velocity profile, which would otherwise be calculated by averaging velocities, in terms of segment lengths of displacements. This is shown to greatly reduce statistical error and allow the flow velocity profile to be calculated using very sparse time sampling. In section 3, we consider the same physical problem treated with linear response theory. The Green−Kubo expression for the velocity profile[23−25] is recast in terms of the mean codisplacements along unwrapped trajectories. Again, the reformulation reduces statistical error and permits very sparse time sampling. A different set of problems is treated in section 4. There, we consider the extraction of frequency-dependent dielectric properties from equilibrium simulations. Reformulation of the expressions for frequency-dependent electrical susceptibility and conductivity in terms of mean-squared dipolar displacement[31] permits robust estimation of dielectric properties. The advantages of using displacements are summarized and discussed in section 5.

2. NONEQUILIBRIUM FLOW AND DISPLACEMENTS WITHIN SLABS

Consider flow between walls perpendicular to the z-direction, as schematically shown in Figure 1. The objective is to obtain the average fluid velocity within the mth slab parallel to the walls. This is given by the sum of velocity observations within that slab, perhaps at regular time intervals, divided by the number of observations.

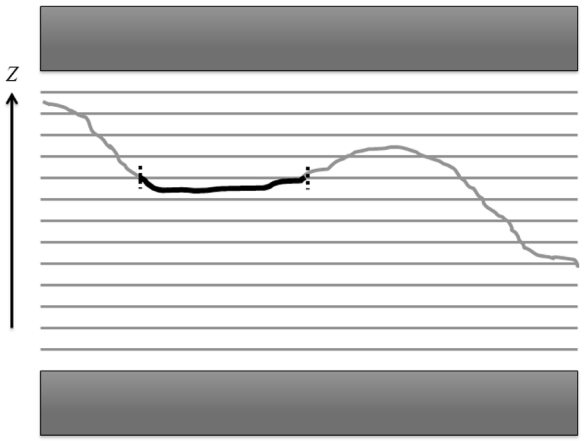

Figure 1. Schematic representation of a channel in which the average flow velocity is calculated within slabs parallel to the walls and perpendicular to the z-direction. A possible particle trajectory is shown, and a heavy line illustrates the segment in which the jth particle enters the mth slab at time $t^{(i)}_{\alpha_{mj}}$ and exits the slab at time $t^{(f)}_{\alpha_{mj}}$. The index α labels the segments into which the trajectory is broken.

$$\mathbf{u}_m = \frac{1}{N_{\mathrm{obs},m}} \sum_{i=1}^{N_{\mathrm{obs},m}} \mathbf{v}_i \tag{1}$$

Velocities are included within the set of $N_{\mathrm{obs},m}$ observations for slab m if the value of z for the particle falls within the slab definition. It is typical that molecular center of mass velocities are of interest for specific chemical species, but subscripts that indicate such choices are suppressed for clarity.

As mentioned in the Introduction, the type of average in eq 1 is subject to large error because the average flow velocity is much less that thermal velocities. Typically, one combines numbers whose magnitude is much greater than the final average. Therefore, $N_{\mathrm{obs},m}$ must be as large as possible, either by frequent sampling or long simulation runs or both. In the limit of continuous sampling, the average flow velocity in slab m becomes a ratio of time integrals.

$$\mathbf{u}_m = \frac{\int_0^T \mathrm{d}t \sum_{j=1}^N \mathbf{v}_j(t) s_m(z_j(t))}{\int_0^T \mathrm{d}t \sum_{j=1}^N s_m(z_j(t))} \tag{2}$$

In eq 2, j is the index of particles, and $s_m(z)$ is the characteristic function for the mth slab. $s_m(z)$ is 1 when z is within slab m and 0 otherwise.

We divide each particle trajectory into segments delimited by entry and exit from a particular slab. The time when the trajectory of particle j enters slab m for the αth time is $t^{(i)}_{\alpha_{mj}}$, and the conclusion of that segment, when the particle leaves for another slab, is $t^{(f)}_{\alpha_{mj}}$. One possible segment is illustrated in Figure 1. The time integrals in eq 2 can be evaluated explicitly in terms of the segment parameters.

$$\mathbf{u}_m = \frac{\sum_{j=1}^N \sum_{\alpha_{mj}} [\mathbf{r}_j(t^{(f)}_{\alpha_{mj}}) - \mathbf{r}_j(t^{(i)}_{\alpha_{mj}})]}{\sum_{j=1}^N \sum_{\alpha_{mj}} [t^{(f)}_{\alpha_{mj}} - t^{(i)}_{\alpha_{mj}}]} \tag{3}$$

dx.doi.org/10.1021/jp5012523 | J. Phys. Chem. B XXXX, XXX, XXX−XXX

The positions in eq 3, being integrals of the velocity, are those of an unwrapped trajectory. The transcription of eq 2 into segments is, in principal, exact and extracts the maximum possible sampling averaging from a molecular dynamics trajectory.

Practical implementation introduces potential approximations because the displacements are not sampled continuously in time but rather at a subset of time points. Very short excursions of a trajectory into a neighboring slab will be missed. It is possible that errors of this type compensate if neighboring slabs borrow segments equally from each other. We employ a linear interpolation between time points to estimate the parameters $t_{\alpha_{mj}}^{(i)}$ and $t_{\alpha_{mj}}^{(f)}$, which is inherently approximate because particle motion is typically diffusive and not ballistic. As the time interval between sample points increases, the quality of the linear interpolation further deteriorates. When the time interval between sample points grows very large, trajectories can cross across multiple slabs between sample points. The list of possible approximations is daunting, but we now provide evidence that these approximations are far from limiting.

Typical results are given here for a model system for electroosmotic flow.[47,48] In the simulation, an electrolyte is confined between charged walls. Because the walls are charged, the electrical double layer near the walls has an opposite charge. An electric field applied parallel to the walls induces electrophoretic motion of the ions. The ions quickly transfer momentum to the fluid as a whole. Because there is a net charge in the fluid, there is a net momentum transfer to the fluid in a direction determined by the direction of the applied field and the net charge in the double layer. The resulting motion of the fluid is electroosmotic flow. The channel walls in our simulation mimic a silicate surface using the interaction potential devised by Lee and Rossky.[49] Water is described with the SPC/E model.[50] The surface area of the silica walls is 3.5nm × 3.4641nm, and the height of the system is 10.0nm. Molecular dynamics simulations are implemented using the GROMACS package.[26,51−53] The walls are given a uniform negative charge of −0.784 e nm^{-2}, where e is an elementary charge, by increasing the magnitude of the charge on the silanol oxygens of the Lee−Rossky model from −0.71 to −0.879642 e. In our system, this gives a total wall charge of −19 e, and 19 sodium ions interacting with water according to the potential devised by Dang[54] are introduced. The simulations analyzed in this section were run for 10 ns. The temperature was maintained at 300 K using a Berendsen thermostat[55] with a time constant of 0.3 ps. We also ran most simulations with a Nosé−Hoover thermostat[56−58] and found no substantial difference. The Lee−Rossky model is not a realistic interaction potential for the charged surface of either a crystalline silicate or amorphous silica. In fact, we have devoted considerable effort to more realistic modeling the water−amorphous silica interface.[22,59,60] The simplified model is used in this study to assess our methods in the absence of other complicating factors.

Figure 2 shows that for the same sparse number of sample points along a trajectory, employing displacements in eq 3 yields the flow velocity profile with far less statistical error than averaging velocity within slabs. With respect to Figure 2, the periodic boundaries were arranged so that the solid wall was situated in the middle. Water molecules only infrequently penetrate to bins near or at the walls; therefore, there will always be some bins with very few samples and large errors, as seen in the figure. In this methodological work, we chose to report the calculated flow profile across the entire region. It would be physically meaningful to only report the flow for bins where the density exceeds a given cutoff.

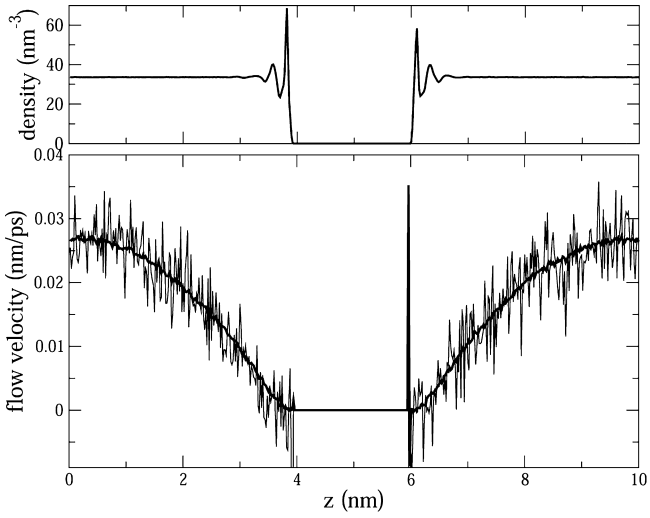

Figure 2. (bottom) Water flow velocity profile for electroosmotic flow in a channel with negatively charged walls and compensating sodium ions. (See the text for further details.) The velocity profiles were calculated either by averaging the center of mass velocities of water molecules within slabs according to eq 1 (thin noisy curve) or breaking the trajectory into segments within slabs and accumulating those segments according to eq 3 (thick smooth curve). The same number of sample points, every 10 ps, were used for both cases. As expected, for the same sampling frequency, accumulating displacements within slabs produces a velocity profile with far less statistical error. (top) The water density. The inner density peaks are not identical at the two surfaces because they are very sharp and align differently with the bins.

Figure 3 addresses possible error that the segment formula could incur if the time interval between sample points is too large. When the sampling interval is 10 or 20 ps, the results are indistinguishable from a very small sampling interval of 0.1 ps. When the sampling interval rises to 30 ps, at which point water molecules in the center of the channel are flowing nearly one-fourth of the box length between sampling times, some error is apparent.

3. FLOW VELOCITY FROM LINEAR RESPONSE THEORY AND CODISPLACEMENTS

In nonequilibrium calculations, a large applied field is desirable to obtain the best signal-to-noise. This is especially true for flow velocity, which must be small compared to thermal velocities for the system to be in the linear response regime. Ideally, more than one external field strength should be tested to check linearity. The same flow profile obtained from nonequilibrium molecular dynamics in section 2 can be calculated from linear response theory.[61−65] The Green−Kubo approach has been developed for the case of electroosmotic flow by Marry, Dufreche, and co-workers.[23−25] To date, this implementation is hampered by insufficient sampling. For example, the error bars in Figure 5 of ref 25 are roughly 1/3 of the flow velocity, and the profile is calculated within only 3−8 slabs, not offering much detail about the flow velocity profile. (Compare to the number of bins in Figures 2 and 3.) In this section, we demonstrate that by using displacements, we can greatly improve sampling for the time correlation functions required for the linear response expressions. We find that, for

dx.doi.org/10.1021/jp5012523 | J. Phys. Chem. B XXXX, XXX, XXX−XXX

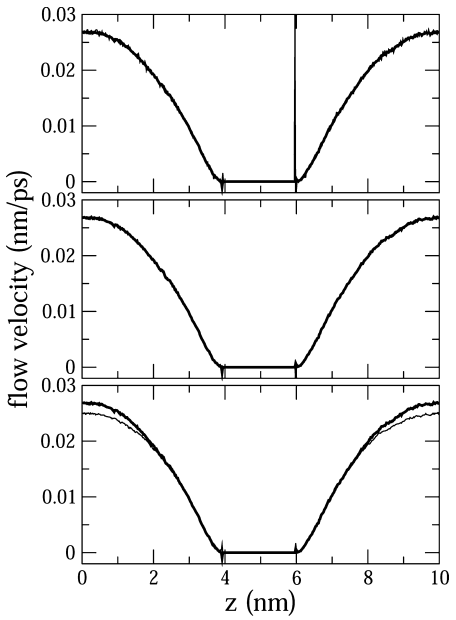

Figure 3. Electroosmotic flow profile in the same system as that of Figure 2. The flow profile is calculated by accumulating segments using eq 3. From top to bottom, the flow velocity calculated using a sampling interval of 0.1 ps (thick curve) is compared with the flow velocity calculated with a sampling interval of 10, 20, and 30 ps. For sampling intervals of 10 and 20 ps, the curves are virtually indistinguishable except for a bin at the surface of the solid layer.

comparable effort, linear response has greater statistical error than nonequilibrium molecular dynamics. However, sufficient accuracy is possible to, for example, clearly establish whether the nonequilibrium calculations were in the linear response regime.

Consider a perturbing potential turned on at time $t = 0$ that drives particle j in the direction $\mathbf{g}_j$.

$$-F\theta(t)\sum_{j=1}^{N}\mathbf{g}_j\cdot\mathbf{r}_j \tag{4}$$

In the above equation, F is an arbitrary field strength, and $\theta(t)$ is the usual step function. Poiseuille flow is induced by choosing $\mathbf{g}_j = \mathbf{g}$, independent of j. Electroosmotic flow is induced by applying an electric field, for example, if we take the electric field in the x-direction, choose $\mathbf{g}_j = q_j\hat{x}$ and $F = E_x$, where q_j is the charge of particle j, $\hat{x}$ is a unit vector in the x-direction, and E_x is the magnitude of the field. The response of interest is the velocity density. The velocity and number density define the local fluid flow velocity through the following relation.

$$\langle\sum_{k=1}^{N}\mathbf{v}_k\delta(\mathbf{r}_k-\mathbf{r})\rangle = \rho(\mathbf{r})\mathbf{u}(\mathbf{r}) \tag{5}$$

One may alternatively use the momentum density and the mass density to define the flow velocity. Standard linear response theory tells us that the steady-state flow velocity that develops at time $t \to \infty$ is given by the following expression.

$$\begin{aligned}\mathbf{u}(\mathbf{r}) &= \frac{\beta F}{\rho(\mathbf{r})}\int_0^\infty \mathrm{d}t\,\langle\sum_{k=1}^{N}\mathbf{v}_k(t)\delta(\mathbf{r}_k-\mathbf{r})\sum_{j=1}^{N}\mathbf{g}_j\cdot\mathbf{v}_j(0)\rangle\\ &= \frac{\beta F}{\rho(\mathbf{r})}\int_0^\infty \mathrm{d}t\,\langle\mathbf{V}(\mathbf{r},t)J(0)\rangle\end{aligned} \tag{6}$$

where

$$\mathbf{V}(\mathbf{r},t) = \sum_{k=1}^{N}\mathbf{v}_k(t)\delta(\mathbf{r}_k-\mathbf{r}) \qquad J(t) = \sum_{j=1}^{N}\mathbf{g}_j\cdot\mathbf{v}_j(t) \tag{7}$$

Essentially the same equation was previously derived by Marry, Dufreche, and co-workers,[23−25] who calculated the momentum density, and hence, the mass density appears in the denominator. We have suppressed all indices that refer to chemical species. Equation 6 can be applied to subsets of particles within the system. When applied to a molecular fluid, $\mathbf{v}_j$ represents the velocity of charge sites, and j ranges over all charge sites. If the flow of molecules is of interest, $\mathbf{v}_k$ is the center of mass velocity of the molecular species of interest, and k ranges over all such molecules. We chose the letter J because in the case of electrokinetic phenomena, $J(t)$ is the current in the direction of the applied field.

As in section 2, we consider flow velocity within the mth slab parallel to channel walls. Assuming that the slab is sufficiently narrow for $\rho(\mathbf{r})$ to be replaced by a constant ρ_m

$$\begin{aligned}\mathbf{u}_m &= \frac{\beta F}{\rho_m}\int_0^\infty \mathrm{d}t\,\langle\sum_{k=1}^{N}\mathbf{v}_k(t)s_m(z_k(t))\sum_{j=1}^{N}\mathbf{g}_j\cdot\mathbf{v}_j(0)\rangle\\ &= \frac{\beta F}{\rho_m}\int_0^\infty \mathrm{d}t\,\langle\mathbf{V}_m(t)J(0)\rangle\end{aligned} \tag{8}$$

where

$$\mathbf{V}_m(t) = \sum_{k=1}^{N}\mathbf{v}_k(t)s_m(z_k(t)) \tag{9}$$

Then, we introduce displacements associated with the perturbation and response.

$$M_J(t) = \int_0^t \mathrm{d}t'\,J(t') \tag{10}$$

$$\mathbf{R}_m(t) = \int_0^t \mathrm{d}t'\,\mathbf{V}_m(t') \tag{11}$$

For electrokinetic phenomena, $M_J(t)$ is the translational dipole displacement of the ions introduced by Schröder and Steinhauser,[31] while for other situations like Poiseuille flow, the interpretation is different, but the definition still holds. $\mathbf{R}_m(t)$ is a sum of segment lengths, as we encountered in section 2. Following standard manipulations,[66] the time correlation function in eq 8 can be related to a "codisplacement" of $\mathbf{R}_m(t)$ and $M_J(t)$, a generalization of a mean-squared displacement.

$$\mathbf{u}_m = \frac{\beta F}{\rho_m}\lim_{t\to\infty}\frac{1}{2}\frac{\mathrm{d}}{\mathrm{d}t}\langle\mathbf{R}_m(t)M_J(t)\rangle \tag{12}$$

The same electroosmotic flow between walls described with the Lee−Rossky interaction model considered in section 2 is now treated using linear response theory. The data to be discussed was obtained from a 34 ns trajectory generated in the absence of an applied field. The mean codisplacement $\langle\mathbf{R}_m(t)M_J(t)\rangle$ is reported in Figure 4 for several slabs. The limiting slopes give the linear response theory estimate for the flow velocity for individual slabs. Unlike the nonequilibrium simulations of section 2, where an electric field was applied in the x-direction, the x- and y-directions are equivalent, apart from a small crystalline asymmetry, in equilibrium simulations. Therefore,

dx.doi.org/10.1021/jp5012523 | J. Phys. Chem. B XXXX, XXX, XXX−XXX

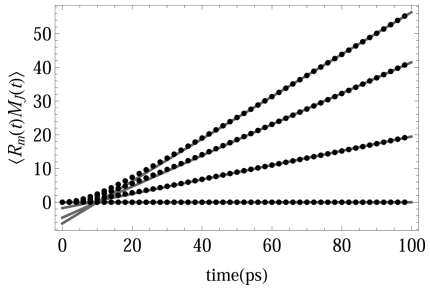

Figure 4. Points in the figure are $\langle \mathbf{R}_m(t)M_J(t)\rangle$ obtained from equilibrium (no applied electric field) simulations of the same system of water and ions confined between walls considered in section 2. The asymptotic slope gives the flow velocity within various slabs parallel to the walls, labeled by the index m, according to eq 12. We chose to illustrate four values of m, ranging from slabs near the channel center, which exhibit the highest slope, to slabs near the channels walls, which have slopes near zero. The gray lines are the fits to large t behavior.

the data in Figure 4 are an average of correlation functions for the x- and y-directions. The top graph of Figure 5 is the flow velocity profile constructed using the linear response expression, eq 12, compared with the nonequilibrium results of section 2. The linear response theory flow profile is approximately one standard deviation from the nonequilibrium results. The bottom graph of Figure 5 provides the flow velocity profile using the velocity−current correlation function of eq 6. Even though the bottom graph is the result of 100 times more sampling points, the error bars of the two linear response estimates are comparable. The statistical error for the linear response profile is larger than than that of the nonequilibrium simulation, despite the fact that a longer trajectory was used to generate the linear response data. Nevertheless, the linear response estimate is valuable because it confirms that the departures from the linear regime in the nonequilibrium simulation are small.

4. DIPOLAR DISPLACEMENTS AND FREQUENCY-DEPENDENT DIELECTRIC PROPERTIES

In the zero-frequency, static limit, the contribution of polar molecules to the dielectric constant can be distinguished from the contribution of ions to the conductivity, although there is a small cross term.[32−35] At finite frequency, the contribution of polar molecules to the frequency-dependent dielectric constant can be distinguished theoretically from the contribution of ions to a frequency-dependent conductivity.[32]

$$\chi_W(\omega) = \epsilon_W(\omega) - \mathbf{1} \tag{13}$$

$$= \frac{\beta}{V\epsilon_0}[\langle \mathbf{M}_W\mathbf{M}_W\rangle + i\omega \int_0^\infty dt\ e^{i\omega t}(\langle \mathbf{M}_W(t)\mathbf{M}_W(0)\rangle + \langle \mathbf{M}_W(t)\mathbf{J}_I(0)\rangle)] \tag{14}$$

$$\sigma_I(\omega) = \frac{\beta}{V}[\int_0^\infty dt\ e^{i\omega t}\langle \mathbf{J}_I(t)\mathbf{J}_I(0)\rangle - i\omega \int_0^\infty dt\ e^{i\omega t}\langle \mathbf{M}_W(t)\mathbf{J}_I(0)\rangle] \tag{15}$$

Here the subscripts W and I denote polar solvent (i.e., water) and ions, respectively, $\mathbf{M}_W$ is the total dipole moment of the polar molecules, $\mathbf{J}_I$ is the total current of the ions, V is the system volume, and ϵ_0 is the vacuum permittivity. χ_W, σ_W, and

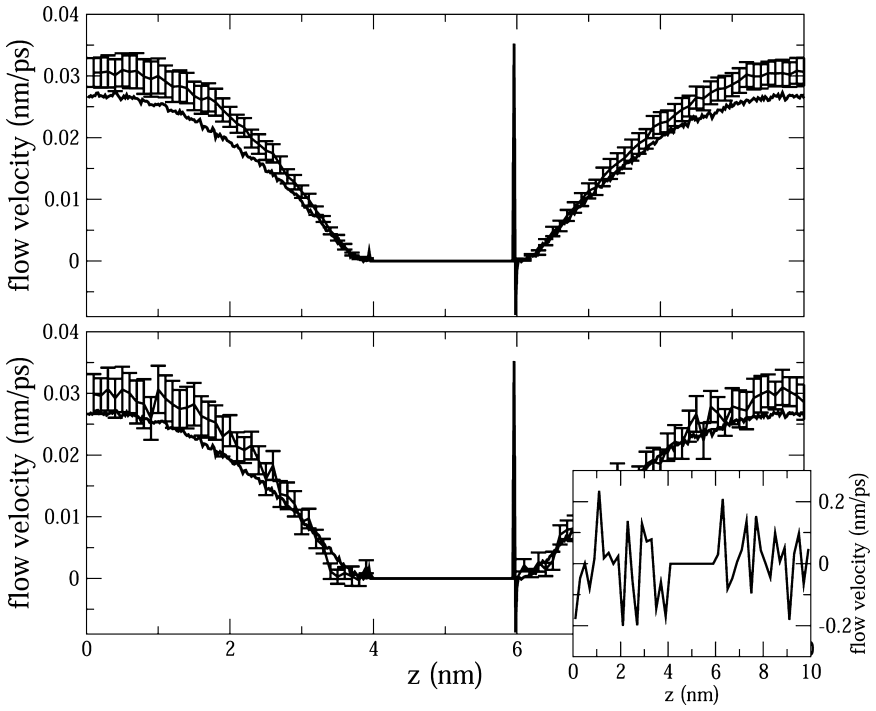

Figure 5. Electroosmotic flow velocity of the same system of water and ions confined between walls considered in section 2. In the full size plots, the flow velocity obtained from nonequilibrium simulations is the heavy black curve without error bars. In the top plot, the flow velocity calculated with linear response theory using the limiting slope of the codisplacement function (eq 12, Figure 4) is shown with error bars corresponding to one standard deviation. The sampling interval was 10 ps. The error bars were calculated using the blocking method[67] with blocks of 2 ns. In the bottom plot, the flow velocity is calculated with linear response theory using a current−velocity correlation function (eq 8, refs 23−25) with a sampling interval of 0.1 ps, that is, 100 times more sampling than the top plot. The inset shows the meaningless velocity profile (note scale) obtained when a sampling interval of 10 ps is used with the current−velocity correlation function.

dx.doi.org/10.1021/jp5012523 | J. Phys. Chem. B XXXX, XXX, XXX−XXX

$\boldsymbol{\epsilon}_W$ are written as tensor quantities. The system under consideration will be isotropic in many situations, and what is accumulated is the average diagonal component of the above expressions. Experimentally, the contribution of polar solvent and ions cannot be separated at finite frequency. That is, $\boldsymbol{\chi}_W(\omega)$ and $\boldsymbol{\sigma}_I(\omega)$ are not separately measurable.[32] An experiment records the overall electric susceptibility $\boldsymbol{\chi}(\omega)$.

$$\boldsymbol{\chi}(\omega) = \boldsymbol{\chi}_W(\omega) - \frac{1}{i\omega\epsilon_0}[\boldsymbol{\sigma}_I(\omega) - \boldsymbol{\sigma}_I(0)] \tag{16}$$

In the same way, the contributions of polar molecules and ions are intertwined at finite frequency in the overall frequency-dependent conductivity and are not separately measurable.

$$\boldsymbol{\sigma}(\omega) = \boldsymbol{\sigma}_I(\omega) - i\omega\epsilon_0\boldsymbol{\chi}_W(\omega) \tag{17}$$

It is common for the overall $\boldsymbol{\chi}(\omega)$ or $\boldsymbol{\sigma}(\omega)$ to be calculated from $\boldsymbol{\chi}_W(\omega)$ and $\boldsymbol{\sigma}_I(\omega)$, and there are practical numerical considerations in favor of this route. However, in principle, the overall susceptibility and conductivity can be obtained from the overall current, $\mathbf{J} = \sum_j q_j\mathbf{v}_j$, including charges on polar molecules.

$$\boldsymbol{\chi}(\omega) = -\frac{\beta}{\epsilon_0 V}\frac{1}{i\omega}\int_0^\infty dt\ (e^{i\omega t} - 1)\langle \mathbf{J}(t)\mathbf{J}(0)\rangle \tag{18}$$

$$\boldsymbol{\sigma}(\omega) = \frac{\beta}{V}\int_0^\infty dt\ e^{i\omega t}\langle \mathbf{J}(t)\mathbf{J}(0)\rangle \tag{19}$$

$\boldsymbol{\chi}(\omega)$ or $\boldsymbol{\sigma}(\omega)$ can be calculated using the dipolar displacement, eq 10, which we accumulate from unwrapped trajectories.

$$\langle \mathbf{M}_J(t)\mathbf{M}_J(t)\rangle = \int_0^t dt' \int_0^t dt''\ \langle \mathbf{J}(|t' - t''|)\mathbf{J}(0)\rangle \tag{20}$$

$$= 2\int_0^t dt'\ (t - t')\langle \mathbf{J}(t')\mathbf{J}(0)\rangle \tag{21}$$

In the above, we used the time invariance property of time correlations functions. The second follows through standard manipulations when the integrand is a function of $|t - t'|$.[66] For full generality, we write these equations in tensor form, although in many cases where the system is isotropic, the average diagonal component is of interest. At long times, the dipolar displacement exhibits diffusive behavior.

$$\lim_{t\to\infty}\langle \mathbf{M}\rangle_J(t)\mathbf{M}_J(t) = \mathbf{A} + \mathbf{B}t \tag{22}$$

In our calculations, the quantities $\mathbf{A}$ and $\mathbf{B}$ are obtained by fitting to the long-time behavior, as we did for the codisplacements in Figure 4.

The relationship between the current−current correlation function and the mean-squared dipolar displacement can be exposed by taking two time derivatives of eq 21.

$$\int_0^t dt'\ \langle \mathbf{J}(t')\mathbf{J}(0)\rangle = \frac{1}{2}\frac{d}{dt}\langle \mathbf{M}\rangle_J(t)\mathbf{M}_J(t) \tag{23}$$

$$\langle \mathbf{J}(t)\mathbf{J}(0)\rangle = \frac{1}{2}\frac{d^2}{dt^2}\langle \mathbf{M}\rangle_J(t)\mathbf{M}_J(t) \tag{24}$$

To work with a function that vanishes as $t \to \infty$, insert $\langle \mathbf{J}(t')\mathbf{J}(0)\rangle = (1/2)(d^2/dt^2)(\langle M_J^2(t)\rangle - \mathbf{A} - \mathbf{B}t)$ into eqs 18 and 19 and integrate by parts. We find two alternative expressions that can be used to extract the electrical susceptibility from equilibrium molecular dynamics simulations.

$$\boldsymbol{\chi}(\omega) = \frac{\beta}{2\epsilon_0 V}\int_0^\infty dt\ e^{i\omega t}\left[\frac{d}{dt}\langle M_J^2(t)\rangle - \mathbf{B}\right] \tag{25}$$

$$\boldsymbol{\chi}(\omega) = \frac{\beta}{2\epsilon_0 V}\{\mathbf{A} - i\omega\int_0^\infty dt\ e^{i\omega t}[\langle M_J^2(t)\rangle - \mathbf{A} - \mathbf{B}t]\} \tag{26}$$

From eq 26, we associate the constant $\mathbf{A}$ with the zero-frequency electrical susceptibility.

$$\boldsymbol{\chi}(0) = \frac{\beta}{2\epsilon_0 V}\mathbf{A} \tag{27}$$

We also find two alternative expressions for the conductivity in a similar fashion.

$$\boldsymbol{\sigma}(\omega) = \frac{\beta}{2V}\left\{\mathbf{B} - i\omega\int_0^\infty dt\ e^{i\omega t}\left[\frac{d}{dt}\langle M_J^2(t)\rangle - \mathbf{B}\right]\right\} \tag{28}$$

$$\boldsymbol{\sigma}(\omega) = \frac{\beta}{2V}\{\mathbf{B} - i\omega\mathbf{A} - \omega^2\int_0^\infty dt\ e^{i\omega t}[\langle M_J^2(t)\rangle - \mathbf{A} - \mathbf{B}t]\} \tag{29}$$

From either of the above equations, we associate the constant $\mathbf{B}$ with the zero-frequency conductivity.

$$\boldsymbol{\sigma}(0) = \frac{\beta}{2V}\mathbf{B} \tag{30}$$

The preceding equations are either explicit or implicit in the work of Schröder and Steinhauser.[31] Schröder has recently employed exponential fitting functions to obtain the frequency-dependent dielectric response from the mean-squared dipole displacement. The dipolar displacement has been compared with the current−current correlation function by Picálek and Kolafa[68] as a means to obtain the zero-frequency conductivity.

Here, we demonstrate that accumulating the mean-squared dipolar displacement for ions is an alternative with greater tolerance for a larger sampling interval than the current−current correlation function. We consider a system of 5648 water molecules and 92 Na^+/Cl^- ion pairs. Water is described by the SPC/E model[50] and ion−water interactions by the potentials of Dang.[54] The system was allowed to equilibrate at 1 bar and 300 K before continuing for 6 ns at fixed volume $(5.5704\ nm)^3$ at which the salt concentration was 0.884 M. The Nosé−Hoover thermostat[56−58] with a time constant of 0.3 ps was employed to maintain the system at 300 K.

The total electrical susceptibility contains a water−water contribution, usually calculated with a dipole−dipole correlation function, an ion−ion contribution, usually calculated with a current−current correlation function, and small cross terms. The total susceptibility $\boldsymbol{\chi}(\omega)$ is dominated by the contribution from water and is not a rigorous test of the ability to work with mean-squared dipolar displacement instead of the current−current correlation function. Here, we focus on the ion−ion term. When implementing the imaginary Laplace transform, the large sampling intervals that we reach are are not sufficient to numerically integrate $e^{i\omega t}$. Therefore, we use a dense grid for the Laplace transform and generate the mean-squared dipolar displacement on the dense grid using a simple cubic spline. (An alternative might be Filon's method,[69,70] to which this procedure is closely related.) As can be seen in Figure 6, both the mean-squared dipolar displacement form (left

dx.doi.org/10.1021/jp5012523 | J. Phys. Chem. B XXXX, XXX, XXX−XXX

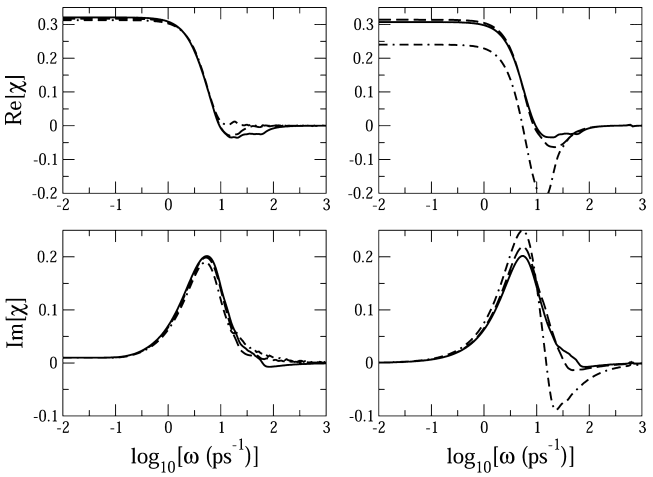

Figure 6. Real and imaginary parts of the ion−ion contribution to $\chi(\omega)$ calculated via the mean-squared dipolar displacement of ions (left column) and via the current−current correlation function (right column). The left and right columns were calculated using eqs 26 and 18, respectively. The solid, dashed, and dotted−dashed curves are the result of using an interval between sampling points of 0.01, 0.1, and 0.2 ps, respectively.

column) and current−current correlation function form (right column) are fairly tolerant to extending the sampling interval to 0.1 ps. The current−current results begin to degrade with a sampling interval of 0.2 ps, while the mean-squared dipolar displacement is not strongly affected.

For a simple electrolyte like the one considered here, the current−current correlation function of the ions is quite short-ranged in time, and relatively short simulations are adequate to obtain convergence. However, the current−current correlation function of charged biomolecules is expected to be long-ranged in time, and moving to the mean-squared dipolar displacement form, eqs 25 and 26, may be advantageous. These results are exploratory, and a more definitive evaluation of the methods must await application to large ions, like DNA, where slow dynamics are expected. Here, we explore the feasibility of generating the ion−ion contribution to $\chi(\omega)$ using the mean-squared dipolar displacement of ions.

5. SUMMARY AND CONCLUSIONS

At present, there is a range of systems where continuum theories for nonequilibrium phenomena can be compared with detailed molecular dynamics simulations. This overlap has provided valuable insights for bridging from molecular to mesoscopic phenomena. In the future, as computational capabilities increase, we expect that increasingly larger and more complex systems will be amenable to detailed molecular calculations. Areas where large-scale calculations are in high demand are micro- and nanofluidic biomedical devices and biological systems. This work addresses the challenges of extracting nonequilibrium and transport properties from the very large data sets associated with large-scale molecular dynamics simulations.

The limit of averaging a time series of a current over an increasing fine grid is a time integral of the current, namely, a displacement. The required displacements are associated with unwrapped trajectories. Hence, the unifying thread in the applications here to nonequilibrium flow and dielectric relaxation is the use of displacements to maximize the amount of statistical averaging to be extracted from a simulation with a minimum of sampling from the trajectory.

In this work, we have developed very efficient means to calculate the flow velocity with greater accuracy and using orders of magnitude less sampling from a trajectory than that from conventional methods. We have demonstrated the approach for electroosmotic flow in a slit pore with planar walls. The very same techniques can also be applied, and we have already done so in our lab, to fluid flow in a cylindrical pore. Application to more complex pore geometries will present further challenges. We have illustrated the method for nonequilibrium molecular dynamics and also for the linear response approach to the flow velocity profile. Previous attempts to extract the flow velocity from equilibrium simulations did not yield a sufficiently detailed profile that could be compared with nonequilibrium results. Here, we find that they agree to within approximately one standard deviation of the linear response theory data.

We have also explored the use of dipolar displacements to calculate the frequency-dependent dielectric properties of ions. Instead of using a current−current correlation function, as is conventionally done, we employ the integrated ion current, the dipolar displacement. We find that for small ions, by working with the mean-squared dipolar displacement instead of the current−current correlation function, one can proceed to a larger sampling interval with less error. However, the goal is to describe dielectric relaxation of large, charged biomolecules. To date, dielectric relaxation of large biomolecules,[31,43] and even smaller biomolecules like amino acids,[44] has been extracted from simulations by fitting simulation data to analytic forms such as multiple exponentials or a stretched exponential. It would be desirable to directly treat simulation data instead of using a preconceived fitting form. The present efforts are only a preliminary step in that direction, and further development is needed before large biomolecules can be handled on the same footing as simple electrolyte solutions.

AUTHOR INFORMATION

Corresponding Author

*E-mail: singer@chemistry.ohio-state.edu. Phone: 614-292-8909.

Notes

The authors declare no competing financial interest.

ACKNOWLEDGMENTS

This work was supported by the National Science Foundation Grant EEC-0914790. The calculations reported here were made possible by a grant of resources from the Ohio Supercomputer Center.

REFERENCES

(1) Travis, K. P.; Todd, B. D.; Evans, D. J. Poiseuille Flow of Molecular Solids. *Physica A* **1997**, *240*, 315−327.

(2) Mansour, M. M.; Baras, F.; Garcia, A. L. On the Validity of Hydrodynamics in Plane Poiseuille Flows. *Physica* **1997**, *A240*, 255−267.

(3) Tuckerman, M. E.; Mundy, C. J.; Balasubramanian, S.; Klein, M. L. Modified Nonequilibrium Molecular Dynamics for Fluid Flows with Energy Conservation. *J. Chem. Phys.* **1997**, *106*, 5615−5621.

(4) Lyklema, J.; Rovillard, S.; Coninck, J. D. Electrokinetics: The Properties of the Stagnant Layer Unraveled. *Langmuir* **1998**, *14*, 5659−5663.

(5) Travis, K. P.; Gubbins, K. E. Poiseuille Flow of Lennard-Jones Fluids in Narrow Slit Pores. *J. Chem. Phys.* **2000**, *112*, 1984−1994.
(6) Freund, J. B. Electro-osmosis in a Nanometer-Scale Channel Studied by Atomistic Simulation. *J. Chem. Phys.* **2002**, *116*, 2194−2200.
(7) Zhu, W.; Singer, S. J.; Zheng, Z.; Conlisk, A. T. Electroosmotic Flow of a Model Electrolyte. *Phys. Rev. E* **2005**, *71*, 041501.
(8) Qiao, R.; Aluru, N. R. Ion Concentrations and Velocity Profiles in Nanochannel Electroosmotic Flows. *J. Chem. Phys.* **2003**, *118*, 4692−4701.
(9) Joly, L.; Ybert, C.; Trizac, E.; Bocquet, L. Hydrodynamics within the Electric Double Layer on Slipping Surfaces. *Phys. Rev. Lett.* **2004**, *93*, 257805.
(10) Qiao, R.; Aluru, N. R. Charge Inversion and Flow Reversal in a Nanochannel Electro-osmotic Flow. *Phys. Rev. Lett.* **2004**, *92*, 198301.
(11) Joly, L.; Ybert, C.; Trizac, E.; Bocquet, L. Liquid Friction on Charged Surfaces: From Hydrodynamic Slippage to Electrokinetics. *J. Chem. Phys.* **2006**, *125*, 204716.
(12) Joseph, S.; Aluru, N. R. Hierarchical Multiscale Simulation of Electrokinetic Transport in Silica Nanochannels at the Point of Zero Charge. *Langmuir* **2006**, *22*, 9041−9051.
(13) Kim, D.; Darve, E. Molecular Dynamics Simulation of Electro-osmotic Flows in Rough Wall Nanochannels. *Phys. Rev. E* **2006**, *73*, 051203.
(14) Lorenz, C. D.; Travesset, A. Charge Inversion of Divalent Ionic Solutions in Silica Channels. *Phys. Rev. E* **2007**, *75*, 061202.
(15) Lorenz, C. D.; Crozier, P. S.; Anderson, J. A.; Travesset, A. Molecular Dynamics of Ionic Transport and Electrokinetic Effects in Realistic Silica Channels. *J. Phys. Chem. C* **2008**, *112*, 10222−10232.
(16) Sofos, F. D.; Karakasidis, T. E.; Liakopoulos, A. Effects of Wall Roughness on Flow in Nanochannels. *Phys. Rev.* **2009**, *E79*, 026305.
(17) Liu, C.; Li, Z. Flow Regimes and Parameter Dependence in Nanochannel Flows. *Phys. Rev. E* **2009**, *80*, 036302.
(18) Hansen, J. S.; Todd, B. D.; Daivis, P. J. Prediction of Fluid Velocity Slip at Solid Surfaces. *Phys. Rev. E* **2011**, *84*, 016313.
(19) Kannam, S. K.; Todd, B. D.; Hansen, J. S.; Daivis, P. J. Slip Flow in Graphene Nanochannels. *J. Chem. Phys.* **2011**, *135*, 144701.
(20) Kannam, S. K.; Todd, B. D.; Hansen, J. S.; Daivis, P. J. Slip Length of Water on Graphene: Limitations of Non-equilibrium Molecular Dynamics Simulations. *J. Chem. Phys.* **2012**, *136*, 024705.
(21) Kannam, S. K.; Todd, B. D.; Hansen, J. S.; Daivis, P. J. Interfacial Slip Friction at a Fluid−Solid Cylindrical Boundary. *J. Chem. Phys.* **2012**, *136*, 244704.
(22) Zhang, H.; Hassanali, A. A.; Shin, Y. K.; Knight, C.; Singer, S. J. The Water−Amorphous Silica Interface: Analysis of the Stern Layer and Surface Conduction. *J. Chem. Phys.* **2011**, *134*, 024705.
(23) Marry, V.; Dufrêche, J.-F.; Jardat, M.; Meriguet, G.; Turq, P.; Grun, F. Dynamics and Transport in Charged Porous Media. *Colloids Surf., A* **2003**, *222*, 147−153.
(24) Marry, V.; Dufrêche, J.-F.; Jardat, M.; Turq, P. Equilibrium and Electrokinetic Phenomena in Charged Porous Media from Microscopic and Mesoscopic Models: Electro-osmosis in Montmorillonite. *Mol. Phys.* **2003**, *101*, 3111−3119.
(25) Dufrêche, J.-F.; Marry, V.; Malíková, N.; Turq, P. Molecular Hydrodynamics for Electro-osmosis in Clays: From Kubo to Smoluchowski. *J. Mol. Liq.* **2005**, *118*, 145−153.
(26) van der Spoel, D.; Lindahl, E.; Hess, B., and the GROMACS development team; *Gromacs User Manual* version 4.6.2, 2013; www.gromacs.org.
(27) Theoretical Group, C. B. *VMD User's Guide*, version 1.9.1; Beckman Institute, University of Illinois at Urbana−Champaign: Urbana−Champaign, IL, 2012.
(28) *LAMMPS Users Manual*; Sandia National Laboratories: Albuquerque, NM, 2013.
(29) Caillol, J. M.; Levesque, D.; Weis, J. J. Electrical Properties of Polarizable Ionic Solutions. I. Theoretical Aspects. *J. Chem. Phys.* **1989**, *91*, 5544−5554.
(30) Caillol, J.-M. Comments on the Numerical Simulations of Electrolytes in Periodic Boundary Conditions. *J. Chem. Phys.* **1994**, *101*, 6080−6090.
(31) Schröder, C.; Steinhauser, O. Computational Dielectric Spectroscopy of Charged, Dipolar Systems. *Computational Spectroscopy*; Wiley-VCH: Weinheim, Germany, 2010; pp 279−321.
(32) Caillol, J. M.; Levesque, D.; Weis, J. J. Theoretical Calculation of Ionic Solution Properties. *J. Chem. Phys.* **1986**, *85*, 6645−6657.
(33) Chandra, A.; Wei, D.; Patey, G. N. Dielectric Relaxation of Electrolyte Solutions: Is There Really a Kinetic Dielectric Decrement? *J. Chem. Phys.* **1993**, *98*, 4959−4966.
(34) Chandra, A.; Wei, D.; Patey, G. N. The Frequency Dependent Conductivity of Electrolyte Solutions. *J. Chem. Phys.* **1993**, *99*, 2083−2094.
(35) Chandra, A. Static Dielectric Constant of Aqueous Electrolyte Solutions: Is There Any Dynamic Contribution? *J. Chem. Phys.* **2000**, *113*, 903−905.
(36) Chowdhuri, S.; Chandra, A. Molecular Dynamics Simulations of Aqueous NaCl and KCl Solutions: Effects of Ion Concentration on the Single-Particle, Pair, And Collective Dynamical Properties of Ions and Water Molecules. *J. Chem. Phys.* **2001**, *115*, 3732−3741.
(37) Löffler, G.; Schreiber, H.; Steinhauser, O. The Frequency-Dependent Conductivity of a Saturated Solution of $ZnBr_2$ in Water: A Molecular Dynamics Simulation. *J. Chem. Phys.* **1997**, *107*, 3135−3143.
(38) Zasetsky, A. Y.; Svishchev, I. M. Dielectric Response of Concentrated NaCl Aqueous Solutions: Molecular Dynamics Simulations. *J. Chem. Phys.* **2001**, *115*, 1448−1454.
(39) Schröder, C. Collective Translational Motions and Cage Relaxations in Molecular Ionic Liquids. *J. Chem. Phys.* **2011**, *135*, 024502.
(40) Kell, D. B. Dielectric Spectroscopy of Biological Systems. *ISI Atlas Sci.: Biochem.* **1988**, *1*, 25−9.
(41) Nandi, N.; Bhattacharyya, K.; Bagchi, B. Dielectric Relaxation and Solvation Dynamics of Water in Complex Chemical and Biological Systems. *Chem. Rev.* **2000**, *100*, 2013−2045.
(42) Young, R. D.; Fenimore, P. W. Coupling of Protein and Environment Fluctuations. *Biochim. Biophys. Acta* **2011**, *1814*, 916−921.
(43) Boresch, S.; Höchtl, P.; Steinhauser, O. Studying the Dielectric Properties of a Protein Solution by Computer Simulation. *J. Phys. Chem. B* **2000**, *104*, 8743−8752.
(44) Boresch, S.; Willensdorfer, M.; Steinhauser, O. A Molecular Dynamics Study of the Dielectric Properties of Aqueous Solutions of Alanine and Alanine Dipeptide. *J. Chem. Phys.* **2004**, *120*, 3333−3347.
(45) Schröder, C.; Steinhauser, O. On the Dielectric Conductivity of Molecular Ionic Liquids. *J. Chem. Phys.* **2009**, *131*, 114504.
(46) Schröder, C.; Steinhauser, O. Using Fit Functions in Computational Dielectric Spectroscopy. *J. Chem. Phys.* **2010**, *132*, 244109.
(47) Russel, W. B.; Saville, D. A.; Schowalter, W. R. *Colloidal Dispersions*; Cambridge University Press: Cambridge, U.K., 1989.
(48) Probstein, R. F. *Physicochemical Hydrodynamics*, 2nd ed.; Wiley: New York, 1994.
(49) Lee, S. H.; Rossky, P. J. A Comparison of the Structure and Dynamics of Liquid Water at Hydrophobic and Hydrophilic Surfaces — A Molecular Dynamics Simulation Study. *J. Chem. Phys.* **1994**, *100*, 3334−3345.
(50) Berendsen, H. J. C.; Grigera, J. R.; Straatsma, T. P. The Missing Term in Effective Pair Potentials. *J. Phys. Chem.* **1987**, *91*, 6269−6271.
(51) Van Der Spoel, D.; Lindahl, E.; Hess, B.; Groenhof, G.; Mark, A. E.; Berendsen, H. J. C. GROMACS: Fast, Flexible, And Free. *J. Comput. Chem.* **2005**, *26*, 1701−1718.
(52) Hess, B.; Kutzner, C.; van der Spoel, D.; Lindahl, E. GROMACS 4: Algorithms for Highly Efficient, Load-Balanced, and Scalable Molecular Simulation. *J. Chem. Theory Comput.* **2008**, *4*, 435−447.
(53) Pronk, S.; et al. GROMACS 4.5: A High-Throughput and Highly Parallel Open Source Molecular Simulation Toolkit. *Bioinformatics* **2013**, *29*, 845−854.

(54) Dang, L. X. Mechanism and Thermodynamics of Ion Selectivity in Aqueous Solutions of 18-Crown-6 Ether: A Molecular Dynamics Study. *J. Am. Chem. Soc.* **1995**, *117*, 6954−6960.
(55) Berendsen, H. J. C.; Postma, J. P. M.; van Gunsteren, W. F.; DiNola, A.; Haak, J. R. Molecular Dynamics with Coupling to an External Bath. *J. Chem. Phys.* **1984**, *81*, 3684−3690.
(56) Nosé, S. A Molecular Dynamics Method for Simulations in the Canonical Ensemble. *Mol. Phys.* **1984**, *52*, 255−268.
(57) Nosé, S. A Unified Formulation of the Constant Temperature Molecular Dynamics Methods. *J. Chem. Phys.* **1984**, *81*, 511−519.
(58) Hoover, W. G. Canonical Dynamics: Equilibrium Phase-Space Distributions. *Phys. Rev. A* **1985**, *31*, 1695−1697.
(59) Hassanali, A. A.; Singer, S. J. A Model for the Water/Amorphous Silica Interface: The Undissociated Surface. *J. Phys. Chem. B* **2007**, *111*, 11181−11193.
(60) Hassanali, A. A.; Zhang, H.; Knight, C.; Shin, Y. K.; Singer, S. J. The Dissociated Amorphous Silica Surface: Model Development and Evaluation. *J. Chem. Theory Comput.* **2010**, *6*, 3456−3471.
(61) Green, M. S. Markoff Random Processes and the Statistical Mechanics of Time-Dependent Phenomena. *J. Chem. Phys.* **1952**, *20*, 1281−1295.
(62) Green, M. S. Markoff Random Processes and the Statistical Mechanics of Time-Dependent Phenomena. II. Irreversible Processes in Fluids. *J. Chem. Phys.* **1954**, *22*, 398−413.
(63) Kubo, R. Statistical-Mechanical Theory of Irreversible Processes. I. General Theory and Simple Applications to Magnetic and Conduction Problems. *J. Phys. Soc. Jpn.* **1957**, *12*, 570−586.
(64) Kubo, R. Some Aspects of the Statistical Mechanical Theory of Irreversible Processes. In *Lectures in Theoretical Physics*; Brittin, E., Dunham, L., Eds.; Interscience: University of Colorado: Boulder, CO, 1958; Vol. *1*, pp 120−203.
(65) Zwanzig, R. Time-Correlation Functions and Transport Coefficients in Statistical Mechanics. *Annu. Rev. Phys. Chem.* **1965**, *16*, 67−102.
(66) Berne, B. J.; Pecora, R. *Dynamic Light Scattering: With Applications to Chemistry, Biology, and Physics*; Courier Dover Publications: Mineola, NY, 2000.
(67) Flyvbjerg, H.; Petersen, H. G. Error Estimates on Averages of Correlated Data. *J. Chem. Phys.* **1989**, *91*, 461−466.
(68) Picálek, J.; Kolafa, J. Molecular Dynamics Study of Conductivity of Ionic Liquids: The Kohlrausch Law. *J. Mol. Liq.* **2007**, *134*, 29−33.
(69) Filon, L. N. G. On a Quadrature Formula for Trigonometric Integrals. *Proc. R. Soc. Edinburgh* **1929**, *49*, 38−47.
(70) Abramowitz, M., Stegun, I. A., Eds. *Handbook of Mathematical Functions*; National Bureau of Standards: Washington, DC, 1972; Applied Mathematics Series 55.